ELSEVIER

Biophysical Chemistry 104 (2003) 79–94

Biophysical Chemistry

www.elsevier.com/locate/bpc

Molecular dynamics simulation of the unfolding of the human prion protein domain under low pH and high temperature conditions

Wei Gu, Tingting Wang, Jiang Zhu, Yunyu Shi[1], Haiyan Liu*

Key Laboratory of Structural Biology, University of Science and Technology of China (USTC), Chinese Academy of Sciences (CAS), School of Life Sciences, USTC, Hefei, Anhui 230026, PR China

Received 25 September 2002; received in revised form 25 September 2002; accepted 23 October 2002

Abstract

Four 10-ns molecular dynamics (MD) simulations of the human prion protein domain (HuPrP 125–228) in explicit water solution have been performed. Each of the simulations mimicked a different environment of the protein: the neutral pH environment was simulated with all histidine residues neutral and bearing a ND proton and with other titratable side chains charged, the weakly acidic environment was simulated with all titratable side chains charged, the strongly acidic environment was simulated with all titratable side chains protonated. The protein in neutral pH environment was simulated at both ambient (298 K) and higher (350 K) temperatures. The native fold is stable in the neutral pH/ambient temperature simulation. Through out all other simulations, a quite stable core consisted of 10–20 residues around the disulfide bond retain their initial conformations. However, the secondary structures of the protein show changes of various degrees compared to the native fold, parts of the helices unfolded and the β-sheets extended. Our simulations indicated that the heat-induced unfolding and acid-induced unfolding of HuPrP might follow different pathways: the initial stage of the acid-induced unfolding may include not only changes in secondary structures, but also changes in the tertiary structures. Under the strongly acidic condition, obvious tertiary structure changes take place after 10-ns simulation, the secondary structure elements and the loops becoming more parallel to each other, resulting in a compact state, which was stabilized by a large number of new, non-native side chain-side chain contacts. Such tertiary structure changes were not observed in the higher temperature simulation, and intuitively, they may favor the further extension of the β-sheets and eventually the agglomeration of multiple protein molecules. The driving forces for this tertiary structure changes are discussed. Two additional 10-ns MD simulations, one with Asp202 protonated and the other with Glu196 protonated compared to the neutral pH simulation, were carried out. The results showed that the stability of the native fold is very subtle and can be strongly disturbed by eliminating a single negative charge at one of such key sites. Correlations of our results with previous experimental and theoretical studies are discussed.

Keywords: Prion protein domain; Molecular dynamics simulation; Unfolding; Low pH; High temperature

*Corresponding author. Tel.: +86-5513607451.
E-mail address: hyliu@ustc.edu.cn (H. Liu).
[1] yyshi@ustc.edu.cn.

0301-4622/03/$ - see front matter © 2003 Elsevier Science B.V. All rights reserved.
PII: S0301-4622(02)00340-X

1. Introduction

Prion disease comprises a group of transmissible fatal neurodegenerative illness including bovine spongiform encephalopathy in cattle and scrapie in sheep. The human versions include kuru, Creutzfeldt–Jakob disease, Gerstmann–Straussler–Scheinker disease and fatal familial insomnia [1,2]. Deposits of protein aggregates or abnormal fibrils in the brain characterize all of these disorders.

According to the protein-only hypothesis [3], the prion is believed to consist of an oligomeric isoform, PrP^{Sc}, of a host-encoded monomeric cellular prion protein (PrP^{C}). The isoforms are most likely identical in covalent structure [4] while having radically different conformations. While the secondary structure of PrP^{C} consists mainly of α-helices, PrP^{Sc} appears to be rich in β-sheets [5,6]. It is believed that the propagation of the disease can be described according to nucleation-dependent polymerization and/or template-assisted models [7].

It has been of increasing interest to study the pH-induced transition from PrP^{C} to PrP^{Sc}. Spectroscopic data show that the stability and conformation of PrP are strongly pH-dependent [8–12]. An equilibrium unfolding intermediate of HuPrP125–228 that shows spectral characteristics of β-sheet proteins has been identified to be exclusively populated at acidic pH [8]. A compact, highly soluble, monomeric form of human prion protein domain (HuPrP90–231) rich in β-sheets has also been reported to exist at low pH [12]. These β-sheet-rich intermediates seem to act as the possible monomer precursors of the scrapie agent. These results agree with the fact that PrP^{Sc} amyloid accumulates in the endosomal lumen of scrapie-infected cells where pH varies between 4.0 and 6.0 [13]. These data suggest that acidic pH may induce the transition between the conformational states of PrP^{C} and PrP^{Sc}. Furthermore, the propagation of the infectious scrapie agent may occur during endocytosis at acidic pH.

PrP^{C} is a secretary cell surface glycoprotein made up of the residues 23–231, which is attached to the cell membrane via a glycosyl phosphatidylinositol anchor at its C terminus [14]. It has a single disulfide bridge and two glycosylation sites [14]. The three-dimensional NMR structure of the recombinant HuPrP (23–231) has revealed that the N-terminal segment (23–120) of the protein is flexible and disordered, while the C-terminal domain (121–231) forms three α-helices (1, 2, 3) and a short pair of β-sheets [15]. Because the segment 90–120 is protected from protease digestion in PrP^{Sc}, it was believed to adopt a well-defined conformation in the PrP^{Sc} but not in PrP^{C} and appeared to be essential for the transition from PrP^{C} to PrP^{Sc} [16]. Indeed, an acid-induced unfolding intermediate with β-sheet properties has been observed in the fragment 90–231 of recombinant HuPrP during guanidinium chloride-induced unfolding transition [10,11]. However, further experiments revealed that an acid-induced intermediate could also form for the C-terminal domain of HuPrP (121–231) and MoPrP (121–231) without the segment 90–120 [8,9]. Although former experiments supported the existence of an intermediate between PrP^{C} and PrP^{Sc} at low pH, recent work on the folding kinetics of HuPrP90–231 and hydrogen/deuterium exchange measurements on HuPrP suggested that PrP^{Sc} is unlikely to be formed from a kinetic intermediate along the natural folding pathway of PrP^{C} [9,17].

Low pH-induced transition from PrP^{C} to PrP^{Sc} involves a dramatic conformational change, and some key events during the early stage of PrP unfolding may trigger this transition. Molecular dynamics simulation makes it possible to probe the atomic details of the conformation change at low pH, as well as the important events in this process [18,19]. There have been MD simulations performed before to try to discover what underlies the transition, including those by Gsponer et al. [20], Alonso et al. [21] and E1-Bastawissy et al. [22]. These simulations are common in their finding of the high flexibility of the loop 167–171 and the loop between helix 2 and helix 3, and in their focus on Asp178, the site where mutations are involved in the prion diseases.

We chose to study HuPrP (125–228) because of its known NMR structure and available detailed experiment data on it. We focus on how HuPrP125–228 deviates from the native PrP^{C} at acidic pH as well as at higher temperature, what

are the key events during the early stage of HuPrP125–228 unfolding, and the probable mechanism underlying this conformation transition.

We carried out a set of four collateral molecular dynamics simulations: HISA; HISH; PH4; and HEAT, each simulating a different experimental condition. HISA represents the nearly neutral pH condition (Arg, Lys positively charged and Asp, Glu negatively charged); HISH represents the weakly acidic condition (His positively charged based on HISA); PH4 represents the strongly acidic environment (pH < 4; Arg, Lys, His residues positively charged; the other residues uncharged). These simulations were carried out at 298 K. HEAT was the same as HISA except that the temperature of the simulation is 350 K. For each set up a 10-ns MD simulation was performed in explicit water. We calculated the root-mean-square (rms) deviations from the NMR structure of each conformation in the trajectories as functions of simulation time and the atomic positional rms fluctuations. Time evolutions of radius of gyration, hydrophilic and hydrophobic solvent accessible surface areas (SASA), secondary structures and side chain–side chain contacts [23] during the simulations were calculated. The trajectories were also analyzed by the essential dynamics approach [24] and by conformation clustering. To look into the effects of the protonation of individual side chains, we selected Asp202 and Glu196 and carried out two additional simulations with only either of the two side chains protonated compared to the HISA set up. We compared different simulations in terms of the changes in secondary structure elements, tertiary structures, residue–residue contact and obtained some insights into the early events and mechanism of acid-induced PrP unfolding. The comparisons between our results and other simulations [20–22] will be discussed.

2. Materials and methods

The initial structures for all the simulations were based on the NMR structure of human prion protein domain: HuPrP(23–230) (PDB Id code: 1AG2) [15], in which the structure of residues 125–228 are well defined. All the simulations were performed with the GROMOS96 package [29], with analyses carried out using functionalities in GROMACS2.0 [30], WhatIf [31], DSSP [25] and MOLMOL [32].

2.1. MD simulations

Four molecular dynamics simulations were performed. Each of the simulations mimic a different environment of the protein: the neutral pH environment (noted as HISA) were simulated with all histidine residues neutral and bearing a ND proton and with other titratable sidechains charged, the weakly acidic environment (noted as HISH) were simulated with all titratable sidechains charged, the strongly acidic environment (named as PH4) were simulated with all titratable side chains protonated. The protein in neutral pH environment was simulated at both ambient and higher (350 K) temperatures (the latter noted as HEAT). The temperature is kept at 300 K in the HISA, HISH and PH4 simulations.

The GROMOS96 condensed-phase force field [29] and the SPC water model [33] have been used. After the protonation states have been decided, counter-ions were added to neutralize the system and truncated octahedron periodic boundary conditions chosen with a solvent shell of 1.0 nm. Non-bonded interactions have been treated using a twin-range cutoff method with the generalized reaction field corrections [28], short-range interactions within 0.8 nm evaluated every time step, medium-range interactions between 0.8 and 1.4 nm updated every 10-time steps, and corrections corresponding to electrostatic interactions beyond 1.4 nm approximated by the reaction field generated by a dielectric continuum with a dielectric constant of 54. A time step of 2 fs was used in the simulations, covalent bond lengths constrained by the SHAKE [34] algorithm with a tolerance of 10^{-4}. The temperature and pressure were kept constant by weak coupling [35] to external heat and isotropic pressure baths, the relaxation times being 0.1 and 0.5 ps, respectively.

After energy minimization, the following procedure has been used to generate equilibrated protein-solvent systems as starting points of the sampling simulations. A 20-ps simulation was performed at 50 K with a coupling constant of

0.01 ps for both the solute and solvent temperature baths, followed by a series of 20-ps simulations each at 100, 150, 200 and 250 K with the coupling constant of 0.01, 0.05, 0.05 and 0.1 ps, respectively. Then, a 400-ps simulation at 298.15 K was performed. The positions of all non-hydrogen protein atoms were restrained in these preparation simulations, with successively decreasing restraining force constants. The sampling simulations are 10-ns MD simulations with no restraint. Coordinates and energies have been recorded every 0.5 ps.

2.2. Contacts analysis

We carried out the contact analysis to characterize the structural changes in the unfolding simulations. Here we adopted the same definition of contact as in Brooks' work [23]: a contact was defined as being present if the centers of geometry of side-chains of two residues (for residue pairs i, j with $j>i+1$) are with 6.5 Å of each other. The state of each contact is defined by a continuous analog of a step function. The state of a contact, $x(i)$, is 1 if the distance, $d(i)$, between the centers of geometry of the side-chains involved is less than 6.5 Å, and 0 if the distance is larger than 7 Å,

$$x(i)=\frac{1}{1+\exp(20\times(d(i)-6.75))}. \quad (1)$$

The frequency of each contact, $p(i)$ is defined based on the fraction of the time that this contact was present in the trajectory.

3. Results and discussions

Fig. 1a–d and Fig. 2a shows the root-mean-square (rms) positional deviations from the NMR structure as functions of simulation time for the C^{α} atoms in each secondary structure elements and for the 66 C^{α} atoms in all the secondary structures. The rms fluctuations of C^{α} atom positions and the time evolutions of hydrophilic and hydrophobic solvent accessible surface areas (SASA) are examined in Fig. 2b–d. Fig. 3 shows the time evolutions of anisotropic radius of gyration (R_g) during the simulations. Fig. 4 shows the evolutions of the secondary structures calculated by DSSP [25]. The secondary structures at the end of the simulations are summarized in Table 1. We clustered the 20 000 conformations sampled in each simulation (data not shown), and select one representative conformation from the largest cluster sampled within the last 2-ns sections in the simulations for analyses and comparisons. Side chain–side chain contact maps of these representative conformations are examined in Fig. 5, and some important contacts with their frequency of occurrence during the simulations are listed in Table 2 and Table 3.

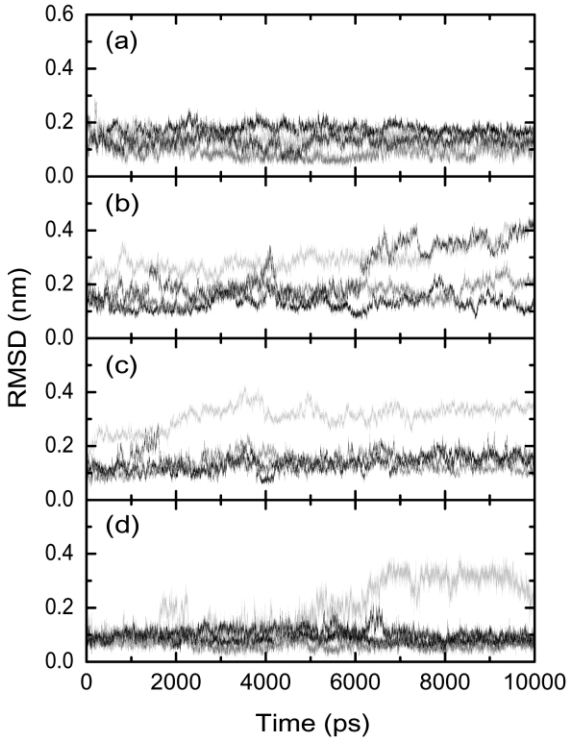

Fig. 1. RMS deviations from the NMR structure as functions of simulation time for C_{α} atoms in secondary structure elements. (a) Helix 1; (b) helix 2; (c) helix 3; (d) β-sheet. Black lines represent the HISA simulation, and red, green and blue lines represent HISH, PH4 and HEAT simulations, respectively.

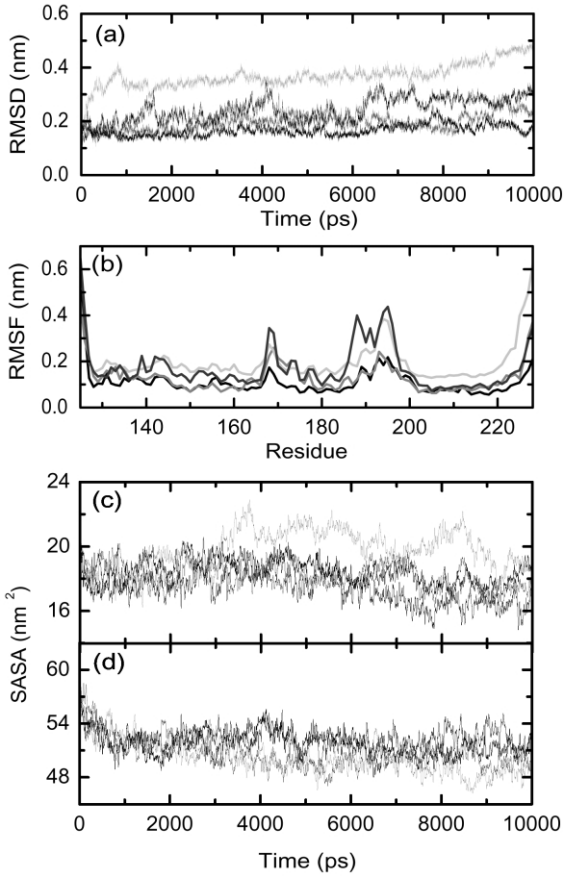

Fig. 2. (a) RMS deviations as functions of time for C_α atoms in all the secondary structures; (b) rms fluctuations of C_α atom positions as functions of residue number; (c) time evolutions of hydrophobic solvent accessible surface areas (SASA); (d) time evolutions of hydrophilic SASA. Black lines represent the HISA simulation, and red, green and blue lines represent HISH, PH4 and HEAT simulations, respectively.

3.1. Overview of the simulations

3.1.1. Structural deviations

Both the acidic and the high temperature environments lead to partial unfolding of the protein in 10 ns. Fig. 2a shows that the HISA simulation, which served as the control, is more stable than other simulations, and the rms deviations are smaller than 0.2 nm in most of the simulation time. In the HISH simulation, the rms deviations are only slightly larger than in the control run. The rms deviations of the HEAT simulations reached 0.28 nm, while the PH4 simulation showed the largest rms deviations that reached 0.45 nm in the 10th nanosecond of the simulation.

3.1.2. Structural fluctuations

Besides the N- and C-terminals of the protein that are highly flexible, there are two conspicuous regions that have significantly larger positional fluctuations than the rest of the protein in all the four simulations: the loop 167–170, and residues 185–200 which include the C-terminal end of helix 2 and its neighboring residues (see Fig. 2b). These two regions, which had larger fluctuation even in the HISA simulation, had also been discussed by Zahn et al. [15]. The higher flexibility of these two loops may indicate the inherent instability of HuPrP.

3.1.3. The hydrophobic core

Despite of the large structural deviations observed in the high temperature and low pH simulations, there is a notable region in the protein that retained its original structure within the simulation time scale. This region consists of a segment located in helix 2 (residues 175–185) in close contact with a segment in helix 3 (residues 210–220). The inter-residue contacts between

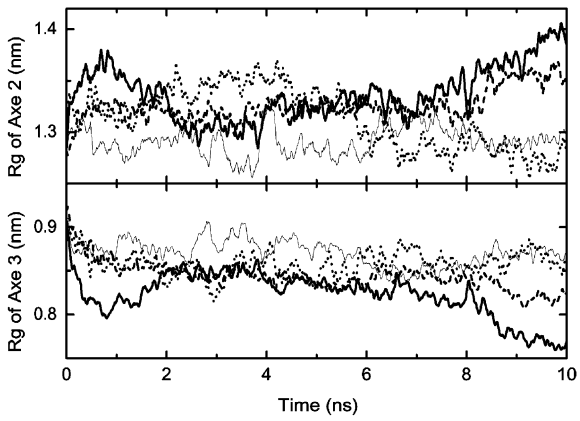

Fig. 3. Time evolutions of the anisotropic radii of gyration (R_g) during the simulations: HISA (thin solid line), HISH (dashed line), PH4 (thick solid line) and HEAT (dotted line).

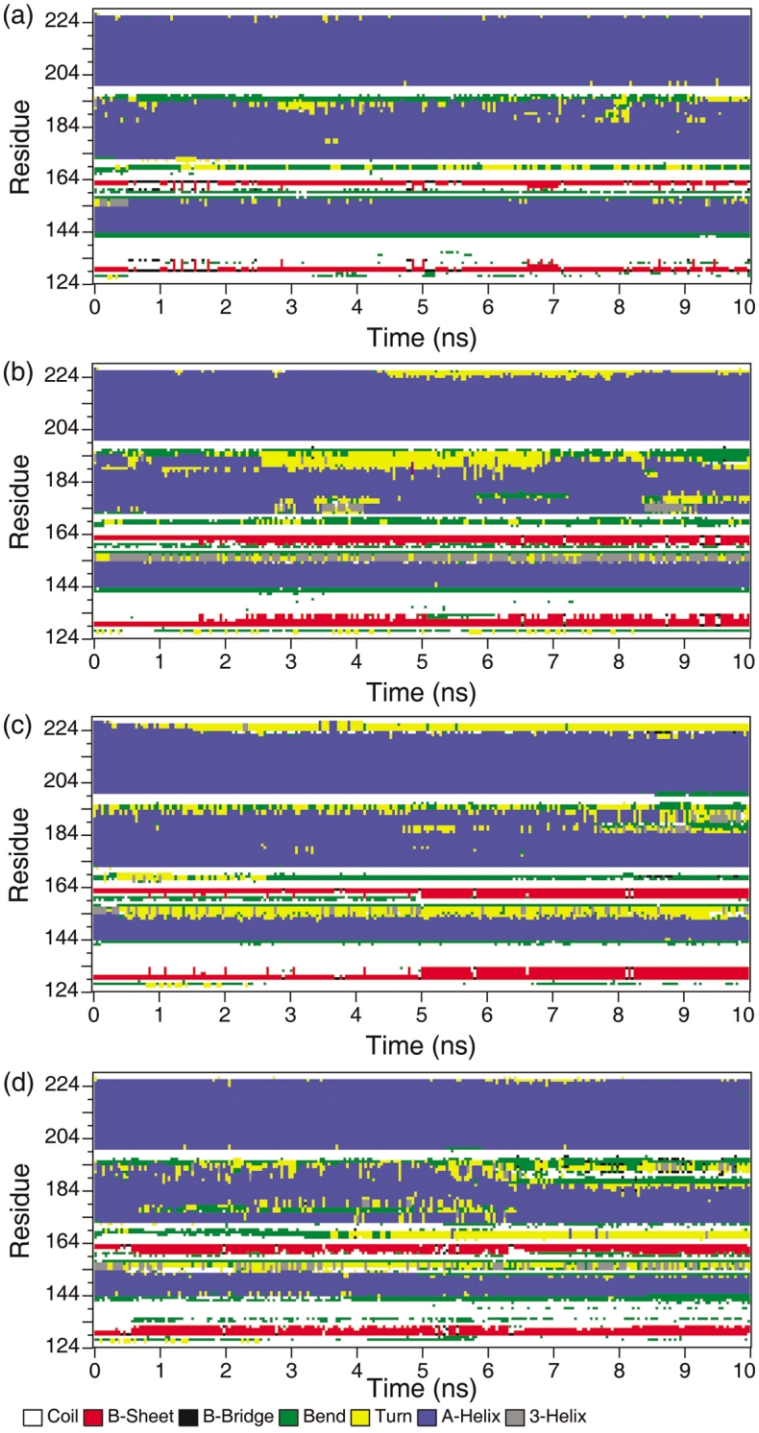

Fig. 4. Secondary structure evolutions as functions of time. (A) HISA; (B) HISH; (C) PH4; and (D) HEAT. The assignments of secondary structures were made with DSSP [25].

Table 1
Secondary structure contents at the end of the simulations

	Helix 1	Helix 2	Helix 3	Sheet
HISA	144–156	173–194	200–226	129–130, 162–163
HISH	144–153	173–176, 179–187	200–225	129–134, 159–163
PH4	144–152	173–184	201–223	129–133, 159–163
HEAT	144–152	173–186	200–226	129–132, 159–163

these two segments are not only dense (Fig. 5), but also stable, having high percentage of occurrence time, as is shown in Table 2, which lists the contacts with high percentage of occurrence (exist within more than 50% of the simulation time). The secondary structures shown in Fig. 4 and the rms fluctuations in Fig. 2b also indicate the higher stability of this region. The conformation of this region is not only stabilized by the disulfide bridge between Cys179 and Cys214, but also by hydrophobic interactions between a number of hydrophobic residues. The higher stability displayed by this region in our simulations is in agreement with an earlier experimental study on HuPrP by Zhang et al., who have identified the region as a 'stable core' [10].

3.1.4. Surface areas

While in the HISA simulation, both the hydrophilic SASA (S_{phi}) and the hydrophobic SASA (S_{pho}) remained stable; the simulations under unfolding conditions show obvious changes in both S_{pho} and S_{phi} (Fig. 2c–d). In PH4, the S_{phi} gradually decreased from 58 to 48 nm^2 and S_{pho} increased from 19 nm^2 to approximately 22 nm^2. Experiments on HuPrP90–231 have shown that the denaturation of the protein involves a massive increase in the exposure of hydrophobic surfaces [11]. This is in agreement with the trend observed in the PH4 simulation. However, in the HEAT simulation the changes are not only reversed but also much smaller compared to the PH4 simulation.

3.2. The secondary structures

3.2.1. Extension of the β-sheets at acidic pH and at high temperature

One of the most important results from the simulations is that the β-sheets extended to approximately twice of its original length under the unfolding conditions (Table 1). The HISA simulation did not show obvious changes in the length of the β-sheets. Fig. 4 shows that in the PH4 simulation, the extension of the β-sheets took place at 5 ns and sustained through out the rest of the simulation. In the simulation of HEAT and HISH, the extension occurred earlier, at 0.5 and 2.2 ns, respectively. In a number of experimental studies, the increasing of β-sheet structures during both acid-induced and heat-induced PrP denaturation processes have been observed [8–12]. Our simulations indicate that this conformational conversion may be initiated at very early stage of the transition process.

3.2.2. Loss of helices at acidic pH and at high temperature

While in the HISA simulation, the structures of the helices are well maintained, as shown by their low positional rms deviations (Fig. 1a–c) and the DSSP results (Fig. 4A, Table 1), it is interesting to note that the stability's of different helices are obviously different under the unfolding conditions.

Helix 1 seems to be the most stable secondary structure of the protein. There was no large change in its structure through out all simulations (Fig. 1a, Table 1), the positional rms deviations of helix 1 remaining low. DSSP analysis indicated that in the PH4 simulation there are some distortions of the C terminal 3–4 residues within 500 ps and soon reached an equilibrium. The C-terminal is also slightly distorted in both the HISA and HISH simulations.

Among the helices, helix 2 seems to be most prone to denaturing environments. The helix 2 is unstable both at low pH and at high temperature. At low pH, the rms deviations for helix 2 increased to approximately 0.3 nm within 400 ps and exceed

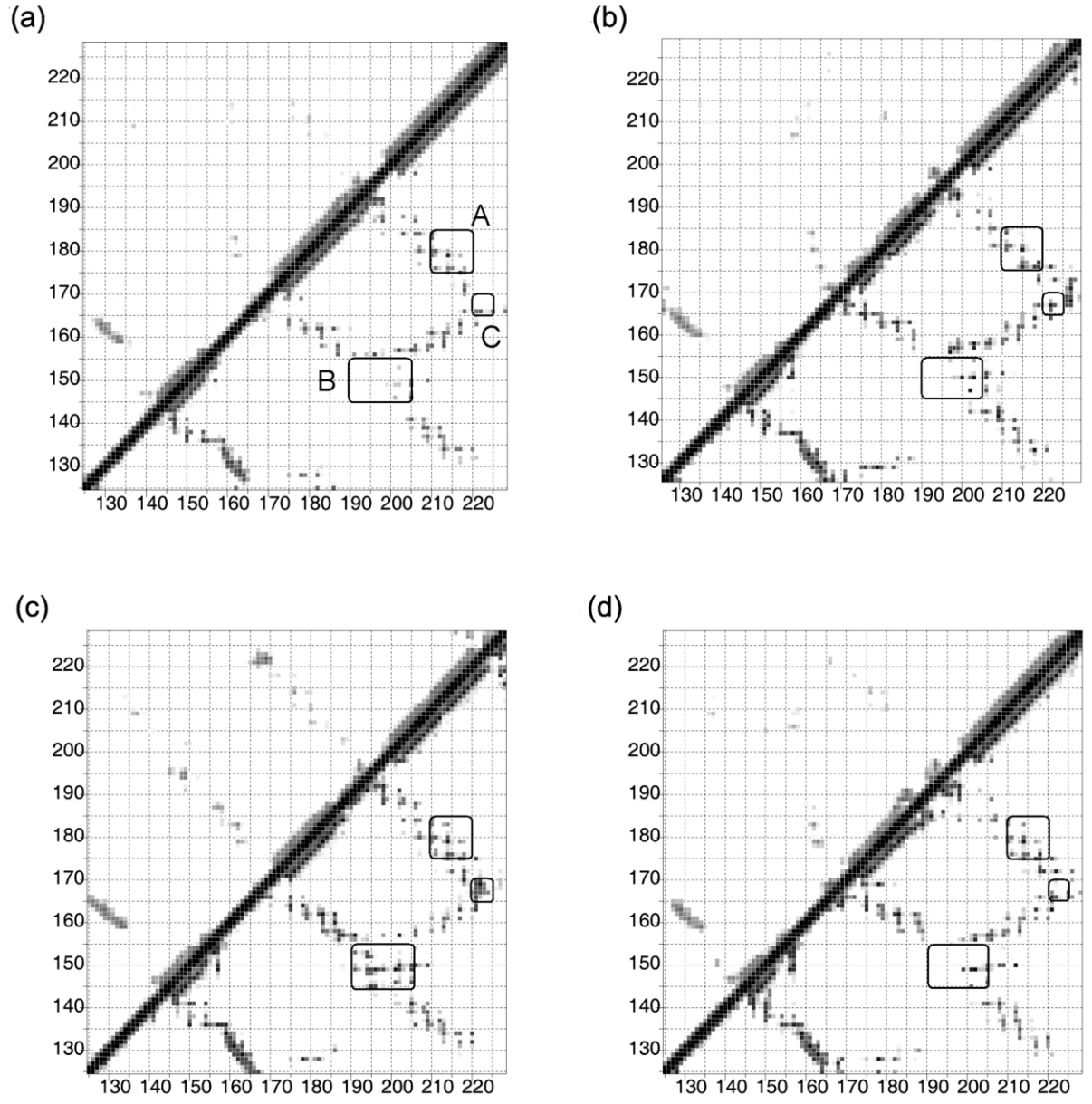

Fig. 5. Residue–residue contact maps for the representative conformations of the largest cluster in the last 2 ns of each simulation. (a) HISA; (b) HISH; (c) PH4; and (d) HEAT. This figure was generated using MOLMOL [32].

0.4 nm after 4 ns (Fig. 1b). In the high temperature simulation, the same deviations remained low during the first 6 ns and after that increased to 0.4 nm within a short period of simulation time (Fig. 1b). Compared to the HISA simulations, the final length of helix 2 calculated by DSSP was 36% (HEAT) to 45% (PH4, HISH) shorter in the other simulations (Table 1). It is interesting to see that in both the PH4 simulation and the HEAT simulation, the unfolding of helix 2 took place at the

Table 2
Side chain–side chain contacts that are well maintained (FREQ > 0.5) in all simulations. The contacts are categorized based on the secondary structure elements to which the side chain belongs

Res. *i*	Res. *j*	FREQ			
		HISA	HISH	PH4	HEAT
Within helix 2					
176	179	0.9877	0.9262	0.7958	0.8416
179	183	0.9532	0.7863	0.7744	0.6346
180	184	0.9192	0.8759	0.5512	0.4933
Within helix 3					
209	213	0.9338	0.9090	0.5048	0.8179
Between helix 2 and helix 3					
176	214	0.9931	0.9561	0.8691	0.7782
176	215	0.9851	0.7902	0.8368	0.7371
179	214	0.9947	0.9572	0.8992	0.7450
180	210	0.9666	0.9608	0.9231	0.7823
180	211	0.9838	0.9667	0.7926	0.7569
180	214	0.9541	0.8434	0.5721	0.6749
183	210	0.9696	0.9368	0.7671	0.6486
184	207	0.9392	0.9390	0.6165	0.6950
184	210	0.9693	0.9172	0.7080	0.6532
Between β-sheets and helix 3					
217	163	0.9057	0.7851	0.7454	0.6323
Within Loops					
166	170	0.9442	0.8184	0.8526	0.6042
Between loops and helix 2					
179	161	0.9774	0.8438	0.8310	0.6614
183	161	0.9759	0.9500	0.8830	0.6745
Between loops and helix 3					
210	161	0.9536	0.9367	0.5417	0.6793
213	161	0.9182	0.9101	0.7864	0.7032
214	161	0.9829	0.9421	0.7796	0.7413

beginning of the simulation (Fig. 4). And at the end of the simulations almost half of the helix had been distorted. The distortion of helix 2 also took place in the HISH simulation.

Helix 3 seems to be unstable only under the low pH condition within the simulation timescale (Fig. 1c, Table 1). In the PH4 simulation, its positional deviations reached 0.3 nm in 2 ns, and in other simulations the same deviations remained to be small.

We suppose that the fragility of helix 2 is related to the intrinsic flexibility of its C-terminal end, as indicated by the positional fluctuation analysis (Fig. 2b). Such flexibility has also been observed by experiments [10–15]. In the NMR structure, there is only one backbone–backbone hydrogen bond (Val189–Thr193) that exists within the C-terminal end (residues 188–194), the other H–O distances between the corresponding NH and CO groups being longer than 3.5 Å, too large for stable hydrogen bonds. We note that the segment 188–194 contains five Thr residues (residues 188, 190, 191, 192 and 193), unfavoring helix formation because of the interactions between their –OH groups and the water molecules.

3.3. The tertiary structure

In the PH4 simulation, a dramatic change in the shape of the protein was observed. This is shown in Fig. 7, in which the conformations from the final sections of the simulations are compared with the NMR structure. The protein was significantly elongated, as indicated by the anisotropic radius of gyration (Fig. 3). In the PH4 simulation, the R_g around the longest axe, axe 2, increased gradually from 1.28 to 1.41 nm (the same value in the HISA and HEAT simulations remains approx. 1.28–1.29 nm.), while the R_g around axe 3 decreased from 0.91 to 0.76 nm (in HISA and HEAT the value was approx. 0.87–0.88 nm). In the HISH simulation, the R_g around axe 2 also increased to 1.35–1.37 nm, and the R_g around axe 3 decreased to 0.82–0.83 nm. From Fig. 7 we can see that the ending conformations from the PH4 simulation is distinct by its narrow, prolonged shape and compact, parallel secondary structures. It is very likely that such a molecular shape favors the formation of β-sheets, which may lead to agglomeration and fibrillation.

The protein at acidic pH is not only elongated, the angles between the roughly parallel backbone segments also becomes smaller. In the PH4 simulation, the angles between helix 1 and helix 3 decreased from 86° to 75°, and the relative positions between the extended loop 3 and helix 3 also changed to be roughly in parallel with each other, resulting in a flatter molecular shape. Loop 1 and loop 2 also tended to be in parallel with each other.

Table 3
Enhanced and new side chain-side chain contacts in the PH4 simulation. The contacts are categorized based on the secondary structure elements to which the side chain belongs. (To be continued in the next page)

Res. *i*	Res. *j*	FREQ	
		PH4	HISA
Within helix 1			
144	147	0.5643	0.1117
146	149	0.5036	0.0064
Within helix 2			
185	189	0.1366	0.0128
175	178	0.1748	0.0010
Within helix 3			
202	206	0.6512	0.0049
204	207	0.2680	0.0465
215	218	0.3605	0.0069
215	219	0.6130	0.1220
205	208	0.4162	0.0402
223	225	0.1433	0.0000
219	227	0.6191	0.0000
222	227	0.5877	0.0294
218	227	0.4675	0.0003
Between helix 1and helix 2			
153	191	0.8351	0.0000
153	187	0.5129	0.0000
152	194	0.1067	0.0000
Between helix 1 and helix 3			
146	205	0.4872	0.0291
146	201	0.7326	0.1255
150	202	0.6065	0.0000
150	206	0.3919	0.0000
Between helix 2 and helix 3			
181	207	0.4179	0.0072
177	211	0.1034	0.0135
191	202	0.1479	0.0000
183	213	0.1738	0.0008
Within β-sheets			
129	163	0.2036	0.0004
130	162	0.1845	0.0348
Between β-sheets and helix 2			
186	130	0.3261	0.0008
Within loops			
139	141	0.6718	0.0997
138	141	0.1824	0.0016
154	157	0.4756	0.0012
165	167	0.2506	0.0168
164	166	0.2055	0.0000
196	198	0.6613	0.1016
136	157	0.2466	0.0001
132	161	0.1510	0.0003
Between loops and helix 1			
147	141	0.6587	0.0616
150	136	0.1650	0.0000
151	141	0.3714	0.0003
149	143	0.1088	0.0000
150	157	0.6347	0.0160
151	154	0.1401	0.0297
153	196	0.6712	0.0003
153	198	0.6403	0.0130
149	196	0.3353	0.0000
152	196	0.6277	0.0000
149	198	0.1981	0.0033
145	196	0.1335	0.0000
Between loops and helix 2			
191	156	0.2146	0.0054
183	158	0.6506	0.0457
184	158	0.3828	0.0015
187	156	0.1389	0.0010
190	156	0.1474	0.0001
191	157	0.2009	0.0034
186	158	0.4251	0.0005
186	160	0.1817	0.0000
Between loops and helix 3			
209	139	0.8333	0.0636
205	139	0.5488	0.0000
210	158	0.3664	0.0678
222	170	0.8006	0.0314
227	169	0.1869	0.0003
223	169	0.1307	0.0000
222	169	0.4705	0.0000
221	170	0.2255	0.0000
202	196	0.4151	0.0101
201	198	0.1351	0.0000

The elongated protein is also more compact in terms of the packing of the helices. The shortest distance between helix 1 and helix 3 reduced from 7.05 to 6.07 Å and between helix 3 and helix 2 from 5.60 to 4.78 Å.

To enable further visualization of the tertiary structure changes in the PH4 simulation, we carried out essential dynamics analyses on the simulations, and each of Fig. 6a–d compares the two extreme conformations along the largest essential mode in each of the simulations. While the largest essential modes in the other simulations consist mainly of

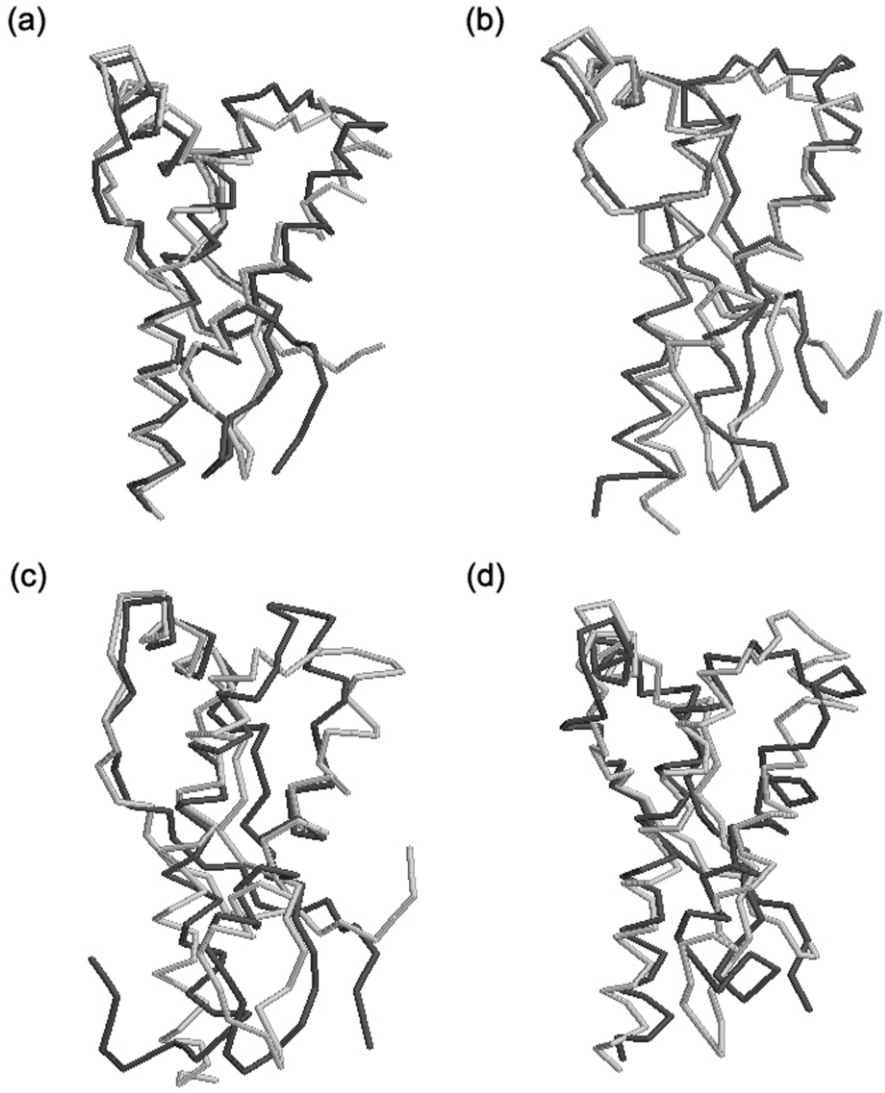

Fig. 6. Extreme structures along the largest eigenvector obtained by essential dynamics analysis of the simulations. (a) HISA; (b) HISH; (c) PH4; and (d) HEAT.

loop motions, the largest essential mode of the PH4 simulation also involves significant changes in the relative orientations of the helices.

The changes in the tertiary structure result in increased interactions between the helices. New contacts occurred between the residues of helices and residues of loops and helices (regions B and C in Fig. 5 and Table 3). Region B in Fig. 5 indicated that in the PH4 simulation, the unfolded C-terminal of helix 2 move towards helix 1 and formed new contacts, while no such new contacts were found in the other simulations. The new contacts formed between the C-terminal of helix 3 and loop 165–170, which were shown as region C in Fig. 5, were also observed only in the PH4 simulation.

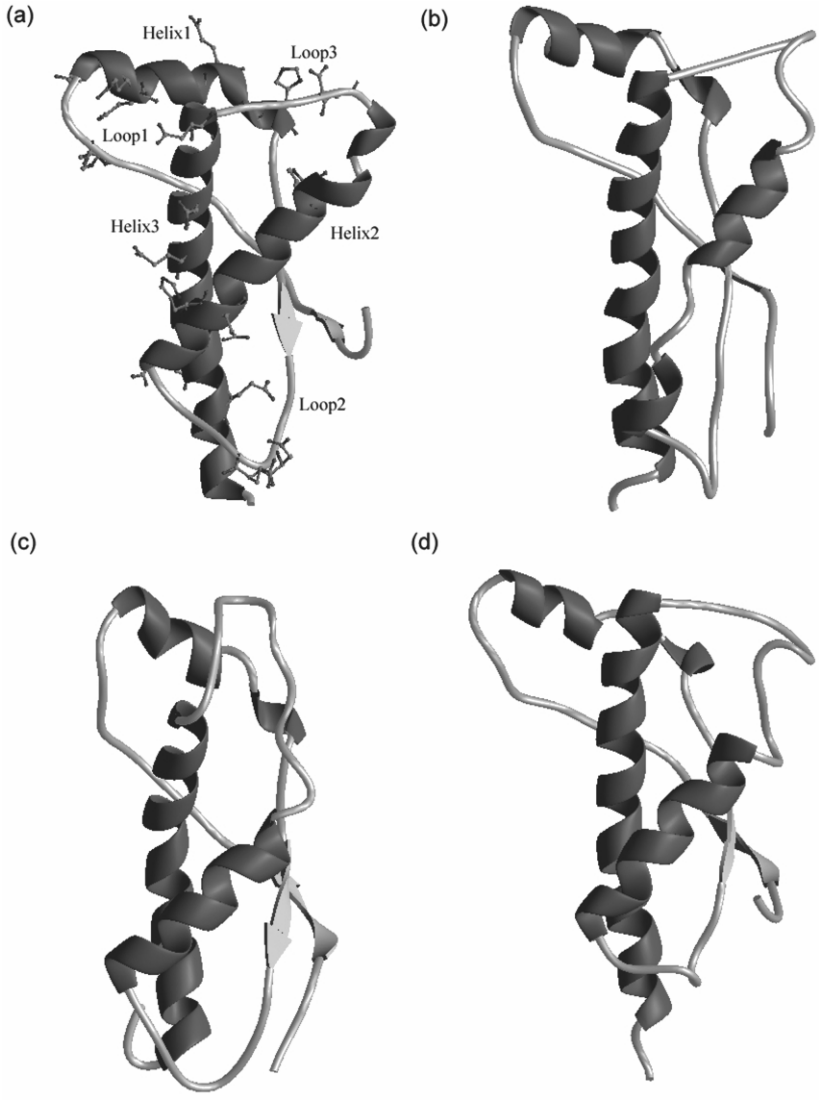

Fig. 7. Schematic ribbon diagrams of the NMR structure and the representative conformations of the largest cluster in the last 2 ns of each simulation. (a) NMR structure; (b) HISH; (c) PH4; and (d) HEAT. In (a), the side chains that are protonated at low pH are shown in a stick representation.

Based on the contact analyses, the tertiary structure changes that took place in the PH4 simulation may be attributed to the following factors: (a) the electrostatic repulsive forces between HD (His140) and HD2 (Asp147) (HD-HD2 distance: 1.9 Å) and between positively charged His140, Arg148 and Arg151 cause the N-terminal end of helix 1 to depart from loop1 (Fig. 7), the entire helix rotating to be in parallel with helix 3; (2) protonation of the Asp and Glu side chains disrupts a number of local interactions in the native tertiary structure, including the hydrogen bonds involving Asp202, Tyr149 and Asn153, and the three salt bridges [26] (Glu146-Arg208, Arg164-Asp178, Arg156-Glu196). Furthermore, protonation eliminates the strong electrostatic repulsive interactions

between Glu196, Glu200, Asp202, Glu146, Glu152, Asp144 and Asp147, which would strongly favor the native tertiary fold over the distorted fold; and (3) the partial unfolding of the C-terminal end of helix 2 leads to the extension of loop 3, increasing the flexibility of the loop, which in turn forms new contacts with helix 1.

3.4. Differences between the acid pH and high temperature simulations

The PH4 simulation, which represents the strongly acidic environment, is much different from the simulation under high temperature condition (HEAT). The PH4 simulation led to not only larger overall rms deviations from the control simulation (Fig. 2b) and shorter helices (Fig. 4 and Table 1), but also distinctive changes in molecular shape (Fig. 2c–d and Fig. 7c–d). The unfolding behaviors of helices 2 and 3 (Fig. 1b–c), especially helix 3, in the low pH and the high temperature simulations are obviously different. The tertiary structure changes that took place in the PH4 simulation were not observed in the HEAT simulation. These results indicate that the acid-induced and high temperature-induced unfolding of HuPrP may have different mechanisms.

3.5. Comparisons with previous MD simulations and the roles of individual residues

A number of simulation studies on the prion protein have been reported previously. Gsponer et al. studied the flexibility of the murine prion protein segment 124–226 and its Asp178Asn mutant under normal pH and temperature condition by MD simulations [20]. To map the early steps in the pH-induced conformational conversion of the Syrian hamster prion protein, Alonso et al. performed a 10-ns MD simulation of residues 109–219 under low pH conditions [21]. El-Bastawissy et al. studied the wild type and a mutant of the human prion protein at both ambient and elevated temperatures (500 K) [22]. Parchment et al. performed MD simulations on mouse and Syrian hamster PrP^C [27]. Zuegg et al. studied the human prion protein, emphasizing the importance of proper treatment of electrostatic interactions in MD simulations [26].

3.5.1. Flexibility of structural segments

High flexibility of the loop 167–171 and the segment connecting Helix 2 and Helix 3, which is found in our simulations, is also reported in the previous studies [20–22,27].

With regard to the flexibility of helix 1, results from different studies are controversial. A study on Syrian hamster PrP^C by Parchment and Essex indicated high flexibility of helix 1, which is not the case in their simulations of mouse PrP^C [27]. They explained this difference as the consequence of the additional unstructured N-terminal region (90–120) in the Syrian hamster PrP^C. However, Gsponer et al. found in their simulations on the mouse protein, which is devoid of the N-terminal region, that helix 1 and its six preceding residues (residues 138–148) are rather flexible [20]. The flexibility of helix 1 was also reported by Alonso et al. who simulated the Syrian hamster PrP^C protein with the unstructured region [21]. Our results on HuPrP without the N-terminal unstructured section are in agreement with the results of Parchment et al., i.e. low flexibility of helix 1, disagree with the results of Gsponer et al. Whether including the N-terminal unstructured region would increase the flexibility of helix 1 remains to be investigated.

3.5.2. Treatment of long-range electrostatic interaction

Zuegg et al. discussed the importance of proper treatment of electrostatic interactions [26]. They reported that the native structure of PrP^C could only be stabilized by treating the long-range electrostatic interactions with the PME method and by neutralizing the system with counter ions in their simulations. Similar results were also reported by El-Bastawissy et al. [22]. In contrast, Alonso et al. and Gsponer et al. both obtained stable trajectories over their simulation time scale at neutral pH by using a cutoff of 10 and 12 Å, respectively [21,22]. In our simulations, we applied the twin-range cutoff method with the generalized reaction field corrections [28]. The reasonable rms devia-

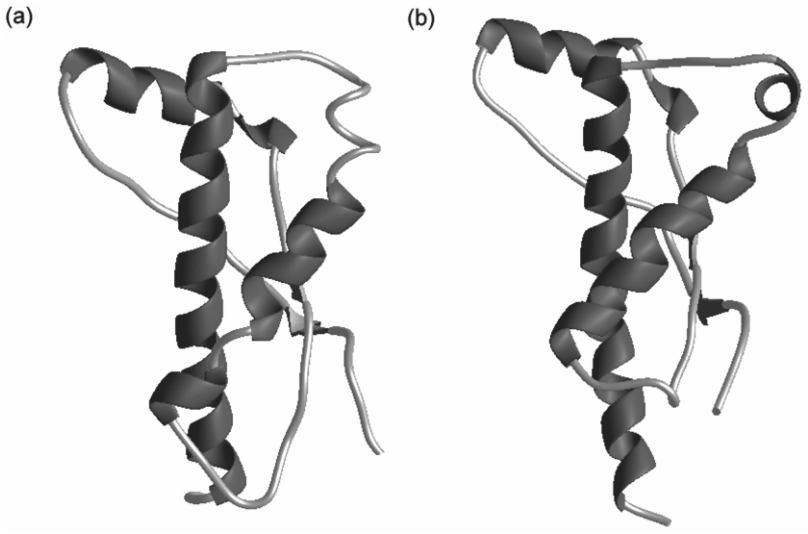

Fig. 8. Schematic ribbon diagrams of the representative conformations of the largest cluster in the last 2 ns of the single site protonation simulations: (a) Glu196; (b) Asp202.

tions of the control run indicate that this treatment is proper for our purpose.

3.5.3. Unfolding at high temperature

The results from El-Bastawissy et al.'s simulations under high temperature [22] showed somewhat difference from ours despite the obvious similarity in the elongation of the β-sheets. The α helices changed little in their simulations, while extensive unfolding of Helix 2 took place in our simulation. We suppose this difference is a result of the different lengths of the simulation time. Their simulation lasted 2 ns, much shorter than the simulation reported here.

3.5.4. Roles of individual residues

In the simulations of human and Syrian hamster PrP^C [26], three salt bridges (Glu146/Asp144–Arg208, Arg164–Asp178, Arg156–Glu196) were reported to be important for the stability of PrP^C. Asp202 was mentioned in Gsponer et al.'s simulation for a salt bridge formed between it and Arg156 [20].

The Asp178Asn mutation was investigated by molecular dynamics simulations in previous studies, but no significant structural changes were observed for this mutant except for a slight increase in the β-sheet content [20–22]. Therefore, the authors suggested that the salt bridge Arg164–Asp178 did not seem to contribute to the overall stability of the $mPrP^C$ [20]. The salt bridge corresponding to Glu146/Asp144-Arg208 does not exist in the domain we studied. We choose to investigate the roles of Glu196 and Asp202 by simulations.

We carried out two 10-ns MD simulations, each with only one of Asp202 and Glu196 protonated compared to the HISA set up. The resulting conformations, noted as Asp202 and Glu196, respectively, both partially reproduced the features of the conformation produced by the PH4 simulation (Fig. 8). The C-terminal end of helix 2 unfolded in both simulations (Fig. 9). In Asp202, the bending of helix 3 can be observed, while in Glu196 the tertiary structure tends to be more compact and elongated without helix 3 bending. The conformational changes in the Glu196 and Asp202 simulations can be explained by the environments where the two residues locate: Asp202 in the native state is attracted to helix 1 by the hydrogen bonds with Tyr149 and Asn153 and is repelled from the C-terminal end of helix 2 by

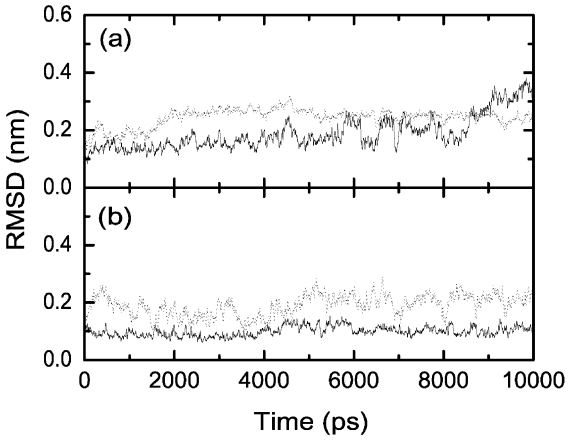

Fig. 9. RMS deviations from the NMR structure as functions of simulation time for C_α atoms in (a) helix 2 and (b) helix 3 in the single site protonation simulations. Dotted lines represent the Glu196 simulation and solid lines represent the Asp202 simulation.

Glu196. Protonation significantly weakens the hydrogen bonds and eliminates the electrostatic repulsion with Glu196. Protonation of Glu196 destroys a salt bridge (Arg156–Glu196) in the native state. Instead, several new contacts between Glu196 and helix 1 were formed at the end of the simulation.

These results indicate that the elimination of even single negative charge may result in significant structure changes in PrP^C. Based on comparisons between the native conformation and the ending conformations of the simulations, negatively charged Glu196 and Asp202 not only play key roles in stabilizing the native conformation, but also may further contribute to the shifting of the conformational equilibrium toward the native state by destabilizing the partially denatured PrP^{SC} state.

4. Conclusions

We have reported MD simulations of a segment (residues 125–228) from HuPrP under different conditions. The simulations are validated and interpreted in light of experimental results in the literature and compared with previous simulations on PrP. Our control simulation well reproduced the native state corresponding to PrP^C. The unfolding of helices and extension of β-sheets were observed in both the low pH and high temperature simulations. However, significant changes in the tertiary structure were only observed in the low pH simulation. Furthermore, the more compact conformation resulted from the low pH simulation, with the overall shape of the protein elongated and the peptide segments in parallel, may favor further extension of the β-sheets. The partial unfolding of helix 2, the extension of loop 3, and the elongation of the tertiary structure may be the early events of the conformational transition process which finally leads to the infectious agent PrP^{Sc}. Our simulations also indicated that the conformational equilibrium is very subtle, eliminating even single negative charge at certain key positions may significantly disturb the native conformation.

Acknowledgments

HY Liu acknowledges financial support from the Chinese National Natural Science Foundation (Grant No. 30025013). YY Shi acknowledges support from the National Basic Research Projects (Grant No. G1999075605) and the Chinese National Natural Science Foundation (Grant No. 39990600). We gratefully thank Professor W.F. van Gunsteren for the GROMOS96 package, Professor H.J.C. Berendsen for the GROMACS2.0 package. We thank ZY Zhang for helping us with the essential dynamics analysis. Some of the figures have been prepared using the Ribbons software [36].

References

[1] S.B. Prusiner, Prion diseases and the BSE crisis, Science 278 (1997) 245.
[2] F.E. Cohen, S.B. Prusiner, Pathologic conformations of prion proteins, Annu. Rev. Biochem. 67 (1998) 793.
[3] J.S. Griffith, Self-replication and scrapie, Nature 215 (1967) 1043.
[4] N. Stahl, M.A. Baldwin, D.B. Teplow, L. Hood, B.W. Gibson, A.L. Burligname, et al., Structural analysis of the scrapie prion protein using mass spectrometry and amino acid sequencing, Biochemistry 32 (1993) 1991.
[5] B.W. Caughey, A. Dong, K.S. Bhat, D. Ernst, S.F. Hayes, W.S. Caughey, Secondary structure analysis of the scrapie-associated protein PrP 27–30 in water by infrared spectroscopy, Biochemistry 30 (1991) 7672.

[6] K.M. Pan, M. Baldwin, J. Nguyen, M. Gasset, A. Serban, D. Groth, et al., Conversion of-helices to-sheets features in the formation of the scrapie prion protein, Proc. Natl. Acad. Sci. USA 90 (1993) 10962.
[7] F.E. Cohen, Protein misfolding and prion diseases, J. Mol. Biol. 293 (1999) 313.
[8] S. Hornemann, R. Glockshuber, A scrapie-like unfolding intermediate of the prion protein domain PrP (121–231) induced by acidic pH, Proc. Natl. Acad. Sci. USA 95 (1998) 6010.
[9] W. Swietnicki, M. Morillas, S.G. Chen, P. Gambetti, W.K. Surewicz, Agrregation and fibrillization of the recombinant human prion protein huPrP90–231, Biochemistry 39 (2000) 424.
[10] H. Zhang, J. Stockel, I. Mehlhorn, D. Groth, M.A. Baldwin, S.B. Prusiner, et al., Physical studies of conformational plasticity in a recombinant prion protein, Biochemistry 36 (1997) 3543.
[11] W. Swietnicki, R. Petersen, P. Gambetti, K. Surewicz, pH-Dependent stability and conformation of the recombinant human prion protein PrP (90–231), J. Biol. Chem. 272 (1997) 27517.
[12] G.S. Jackson, L.P. Hosszu, A. Power, A.F. Hill, J. Kenney, H. Saibil, et al., Reversible conversion of monomeric human prion protein between native and fibrilogenic conformations, Science 283 (1999) 1935.
[13] R.J. Lee, S. Wang, P.S. Low, Measurement of endosome pH following folate receptor-mediated endocytosis, Biochem. Biophys. Acta 1312 (1996) 237.
[14] N. Stahl, S.B. Prusiner, Prions and prion protein, FASEB J. 5 (1991) 2799.
[15] R. Zahn, A. Liu, T. Lûhrs, R. Riek, C.V. Schroetter, F.L. Garcia, et al., NMR solution structure of the human prion protein, Proc. Natl. Acad. Sci. USA 97 (2000) 145.
[16] D. Peretz, R.A. Williamson, Y. Matsunaga, H. Serban, C. Pinilla, R.B. Bastidas, et al., A conformational transition at the N-terminus of the prion protein features in the formation of the scrapie isoform, J. Mol. Biol. 273 (1997) 614.
[17] L.L.P. Hosszu, N.J. Baxter, G.S. Jackson, A. Power, A.R. Clarke, J.P. Waltho, et al., Structural mobility of the human prion protein probed by backbone hydrogen exchange, Nat. Struct. Biol. 6 (1999) 740.
[18] C.M. Dobson, A. Šali, M. Karplus, in: Protein folding: A perspective from theory and experiment, vol 37, Angew. Chem. Int., 1998, p. 868.
[19] S.E. Radford, C.M. Dobson, From computer simulations to human disease. Emerging themes in protein folding, Cell 97 (1999) 291.
[20] J. Gsponer, P. Ferrara, A. Caflisch, Flexibility of the murine prion protein and its Asp178Asn mutant investigated by molecular dynamics simulations, J. Mol. Graphics Model. 20 (2001) 169.
[21] D.O.V. Alonso, S.J. DeArmond, F.E. Cohen, V. Daggett, Mapping the early steps in the pH-induced conformational conversion of the prion protein, Proc. Natl. Acad. Sci. USA 98 (2001) 2985.
[22] E. El-Bastawissy, M.H. Knaggs, I.H. Gilbert, Molecular dynamics simulations of wild-type and point mutation human prion protein at normal and elevated temperature, J. Mol. Graphics Model. 20 (2001) 145.
[23] F.B. Sheinerman, C.L. Brooks III, Calculations on folding of segment B1 of Streptococcal protein G, J. Mol. Biol. 278 (1998) 439.
[24] A. Amadei, A.B.M. Linssen, H.J.C. Berendsen, Essential dynamics of proteins, Proteins 17 (1993) 412.
[25] W. Kabsch, C. Sander, Dictionary of protein secondary structure: pattern recognition of hydrogen-bonded and geometrical features, Biopolymers 22 (1983) 2576.
[26] J. Zuegg, J.E. Gready, Molecular dynamics simulations of human prion protein: importance of correct treatment of electrostatic interactions, Biochemistry 38 (1999) 13862.
[27] O.G. Parchmnet, J.W. Essex, Molecular dynamics of Mouse and Syrian Hamster PrP: implications for activity, PROTEINS, Struct. Funct. Genet. 38 (2000) 327.
[28] I.G. Tironi, R. Sperb, P.E. Smith, W.F. van Gunsteren, J. Chem. Phys. 102 (1995) 5451.
[29] W.F. van Gunsteren, S.R. Billeter, A.A. Eising, P.H. Hunenberger, P. Kruger, A.E. Mark, W.R. Scott, I.G. Tironi, Biomolecular simulation: the GROMOS96 manual and user guide. (Zurich: Vdf Hochschulverlag AG an der ETH Zurich, 1996).
[30] D.van der Spoel, R. van Drunen, H.J.C. Berendsen, Groningen Machine for chemical simulation. (Department of Biophysical Chemistry, BIOSON Research Institute Nijenborgh 4 NL-9717 AG Groningen, 1994).
[31] G. Vriend, WHAT IF: a molecular modelling and drug design program, J. Mol. Graphics 8 (1990) 52.
[32] R. Koradi, M. Billeter, K. Wûthrich, MOLMOL: a program for display and analysis of macromolecular structure, J. Mol. Graphics 4 (1996) 51.
[33] H.J.C. Berendsen, J.P.M. Postma, W.F. van Gunsteren, J. Hermans, Interaction models for water in relation to protein hydration, in: B. Pullman (Ed.), Intermolecular Forces, Reidel, Dordrecht, The Netherlands, 1981, p. 331.
[34] J.P. Ryckaert, G. Ciccotti, H.J.C. Berendsen, Numerical integration of the Cartesian equations of motion of a system with constraints: molecular dynamics of *n*-alkanes, J. Comput. Phys. 23 (1977) 327.
[35] H.J.C. Berendsen, J.P.M. Postma, W.F.v. Gunstereno, A. DiNola, J.R. Haak, Molecular dynamics with coupling to an external bath, J. Chem. Phys. 81 (1984) 684.
[36] M. Carson, R.M. Sweet, C.W. Carter, Ribbons, Methods Enzymol. 277 (1997) 493–505.